Chapter 6

Theoretical Calculations

The differential inclusive multijet event cross-sections measured as a function of $H_{\mathrm{T},2}/2$, described in the previous chapter, are compared with the perturbative QCD (pQCD) theoretical calculations. The lowest order (LO) calculations roughly describe the measured cross-section distributions. The next-to-leading order (NLO) calculations improve the precision by reducing the dependence on the unphysical renormalization (μ_r) and factorization (μ_f) scales. This makes the NLO calculations an essential feature in the determination of fundamental parameters such as α_S and the parton distribution functions (PDFs). This chapter describes the NLO pQCD calculations used for comparison with the cross-section measurements in terms of $H_{\mathrm{T},2}/2$. The NLO pQCD calculations need to be corrected for the multi-parton interactions (MPI) and hadronization effects by applying non-perturbative (NP) corrections and also for the electroweak interactions (EW).

6.1 Fixed Order NLO Calculations

The NLO predictions for the differential inclusive jet event cross-sections in pQCD are computed with the NLOJet++ program version 4.1.3 [67, 68]. As explained in Sec. 3.3.3, the interfacing of NLOJet++ program with fastNLO [69, 70]

framework is preferred over the direct calculation with NLOJET++ because with FASTNLO the calculations of the cross-sections can be repeated for different PDFs and scale choices required for calculating the PDF and scale uncertainties. Here, FASTNLO version 2.3 framework has been used. The PDFs are accessed through the LHAPDF6 library [71, 72]. The factorization and renormalization scales are chosen equal to $H_{\mathrm{T},2}/2$, i.e. $\mu_f = \mu_r = H_{\mathrm{T},2}/2$.

In the current study, the different PDF sets available for a series of different assumptions on the strong coupling constant at the scale of the Z boson mass $\alpha_s(M_Z)$ are used for NLO calculations. Table 6.1 summarizes the existing PDF sets in LHC Run 1 (upper rows) and the newer PDF sets for Run 2 (lower rows). The different columns list the number of flavors N_f, the assumed masses M_t and M_Z of the top quark and the Z boson, respectively, the default values of $\alpha_s(M_Z)$, and the range in $\alpha_s(M_Z)$ variation available for fits with 0.0001 as step size from lowest to highest value. All PDF sets use a variable-flavor number scheme with at most five or six flavors apart from the ABM11 PDF, which employs a fixed-flavor number scheme with $N_F = 5$. Out of these eight PDF sets the following three are not considered further because of the below mentioned reasons :

- At NLO, predictions based on ABM11 do not describe LHC jet data at small jet rapidity [111–114].
- The HERAPDF2.0 set exclusively fits HERA DIS data with only weak constraints on the gluon PDF.
- The range of values available for $\alpha_s(M_Z)$ is too limited for the NNPDF3.0 set.

Mainly CT10 PDF set is considered for comparison between data and theory predictions as well as for calculating theoretical uncertainties.

Table 6.1: NLO PDF sets are available via LHAPDF6 with various assumptions on the value of $\alpha_s(M_Z)$. The upper rows list the existing sets in LHC Run 1 and newer ones for Run 2 are listed in lower rows, along with the corresponding number of flavors N_f, the assumed masses M_t and M_Z of the top quark and the Z boson, respectively, the default values of $\alpha_s(M_Z)$, and the range in $\alpha_s(M_Z)$ variation available for fits.

Base set	N_F	M_t (GeV)	M_Z (GeV)	$\alpha_s(M_Z)$	$\alpha_s(M_Z)$ range
ABM11 [29]	5	180	91.174	0.1180	0.110 - 0.130
CT10 [115]	$\leq$5	172	91.188	0.1180	0.112 - 0.127
MSTW2008 [116, 117]	$\leq$5	10^{10}	91.1876	0.1202	0.110 - 0.130
NNPDF2.3 [118]	$\leq$6	175	91.1876	0.1180	0.114–0.124
CT14 [26]	$\leq$5	172	91.1876	0.1180	0.111–0.123
HERAPDF2.0 [119]	$\leq$5	173	91.1876	0.1180	0.110–0.130
MMHT2014 [27]	$\leq$5	10^{10}	91.1876	0.1200	0.108–0.128
NNPDF3.0 [28]	$\leq$5	173	91.2	0.1180	0.115–0.121

6.1.1 NLO Correction Factors

The ratio of NLO predictions over LO predictions give the effect of the higher-order contributions to the pQCD predictions. These are described by an NLO correction factor, k-factor, which is derived as the ratio of cross-sections as :

$$\text{k-factor} = \frac{\sigma_{\text{NLO}}}{\sigma_{\text{LO}}} \tag{6.1}$$

The impact of the higher-order corrections is determined by the size of k-factor. The small size of k-factor indicates that the cross-section predictions are precisely described at the LO whereas a larger size indicates significant contributions from NLO. Figure 6.1 shows the k-factors of the NLOJET++ calculations, for inclusive 2-jet and 3-jet event cross-sections and their ratio R_{32}, using five different PDF sets. k-factor for R_{32} is obtained by taking the ratio of k-factors for inclusive 3-jet event cross-sections to that of inclusive 2-jet. The k-factors are similar for all the PDF sets in the lower region, but the differences increase in regions with larger $H_{\text{T},2}/2$. It is observed that for inclusive 3-jet event cross-sections, k-factor jumps at the lowest $H_{\text{T},2}/2$. This is because some jet configurations are kinematically forbidden near

the p_{T} cut bin i.e. 150 GeV. Since the first few bins in $H_{\mathrm{T},2}/2$ (below 225 GeV) still suffer from these kinematical constraints, the minimum value of $H_{\mathrm{T},2}/2$ studied is 300 GeV.

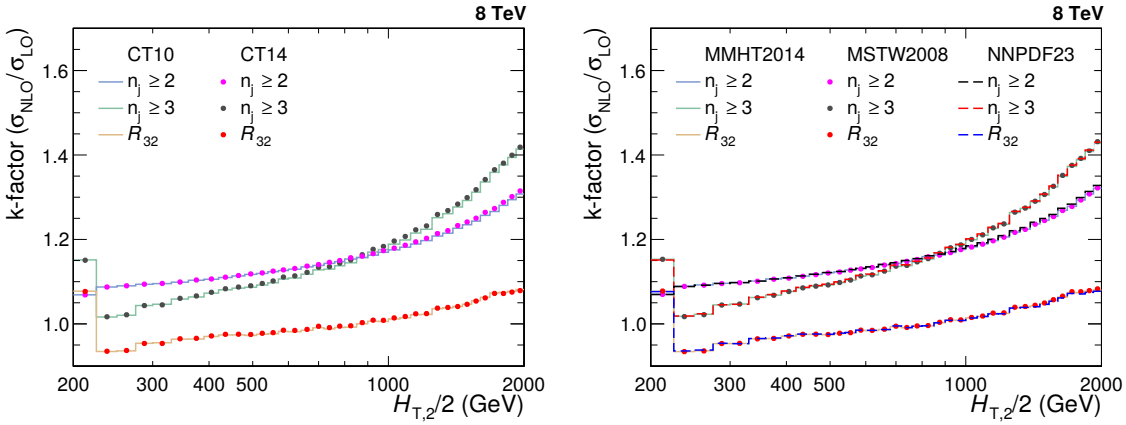

Figure 6.1: The k-factors of the NLOJET++ calculations, for inclusive 2-jet and 3-jet event cross-sections and their ratio R_{32}, using five different PDF sets.

6.1.2 Non-perturbative Corrections

The fixed-order pQCD NLO calculations predict the parton-level cross-section but lack accuracy due to several effects. The partons which are emitted close to each other in phase space are not handled well in the lower order perturbation theories and hence require a parton shower (PS) correction. The scattering phenomena between partons within a colliding proton, other than the hard scattering, give rise to multi-parton interactions (MPI). The partons of the hard scattering form colorless bound states called hadrons through a process of hadronization (HAD). The MPI and hadronization cannot be modelled well within the perturbative framework. Since the fixed-order NLO calculations do not include these additional soft QCD effects, these calculations cannot be compared directly to the unfolded data. Thus corrections for non-perturbative effects (NP) should be taken into account in NLO calculations. The ratio of cross-sections predicted with a nominal event generation, interfaced to the simulation of UE contributions and to the one without hadronization and MPI

effects, gives the NP correction factors which are defined as :

$$C^{\mathrm{NP}} = \frac{\sigma^{\mathrm{PS+HAD+MPI}}}{\sigma^{\mathrm{PS}}} \tag{6.2}$$

In the current study, the NP effects are estimated by using samples obtained from various MC event generators with a simulation of parton shower and underlying-event (UE) contributions. The leading order (LO), HERWIG++ with the default tune of version 2.3 and PYTHIA6 with tune Z2*, and the NLO POWHEG MC event generators are considered. The matrix-element calculation is performed with POWHEG interfaced to PYTHIA8 with tune CUETS1 for the UE simulation. The ratio, defined in Eq. 6.2, is obtained for each MC generator and is fitted by a power-law function defined in Eq. 6.3. Since this ratio obtained from different MC generators have large differences, the average of the envelope, which covers all the differences, is taken as the correction factor which is then applied as bin-by-bin multiplicative factor to the parton-level NLO cross-section. Half of the envelope is taken as the uncertainty on the NP correction factor.

$$f(H_{\mathrm{T},2}/2) = a \cdot \left(H_{\mathrm{T},2}/2\right)^{b} + c \tag{6.3}$$

The NP correction factors, $C^{\mathrm{NP}}_{\text{3-jet}}$ and $C^{\mathrm{NP}}_{\text{2-jet}}$ are calculated for $\mathrm{n_j} \geq 3$ and $\mathrm{n_j} \geq 2$ event cross-sections, respectively and then their ratio gives the correction factor for R_{32}. The correction factors are shown in Fig. 6.2 for the inclusive 2-jet (top left) and 3-jet (top right) event cross-sections, and for the cross-section ratio R_{32} (bottom). At $H_{\mathrm{T},2}/2$ ~300 GeV, the NP corrections amount to ~4-5% for inclusive 2-jet and 3-jet event cross-sections and ~1% for R_{32}, and decrease rapidly for increasing $H_{\mathrm{T},2}/2$. On comparing the NP correction factors of R_{32} with that for individual cross-sections, it has been observed that the non-perturbative effects get reduced in R_{32}.

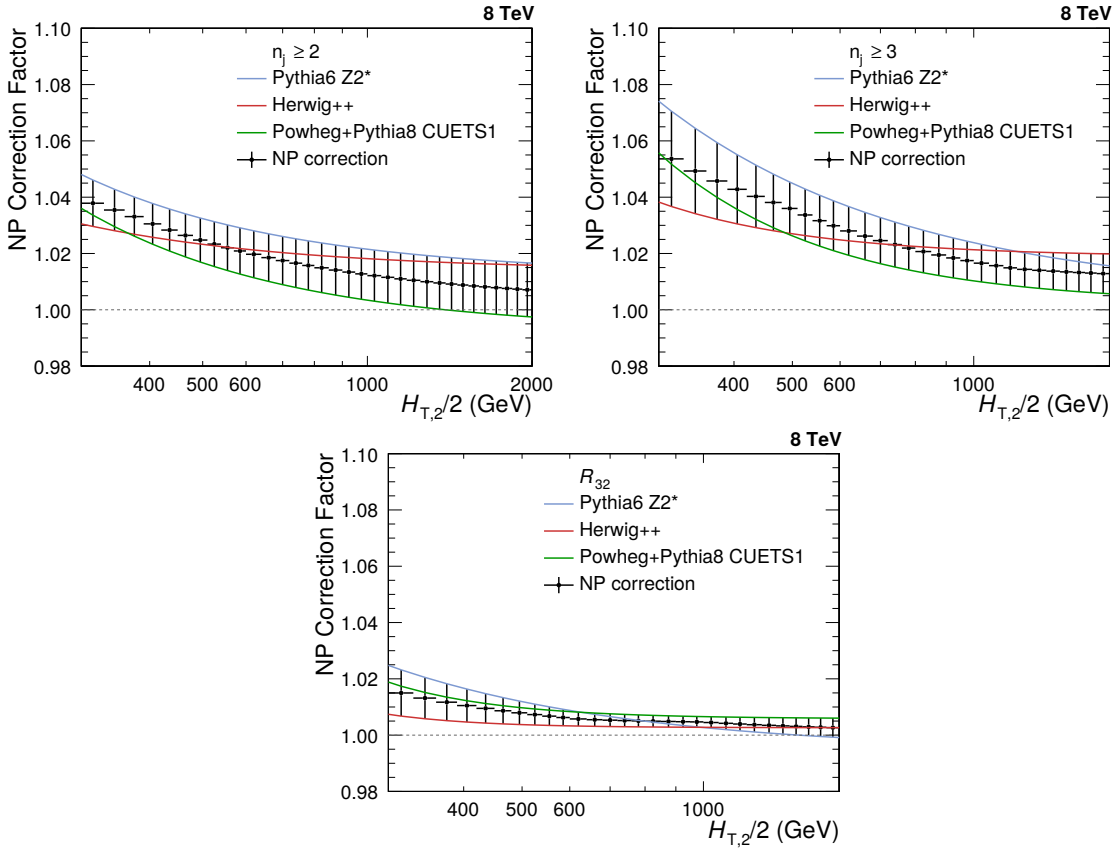

Figure 6.2: The nonperturbative (NP) corrections are presented as a function of $H_{T,2}/2$ for inclusive 2-jet (top left) and 3-jet (top right) event cross-sections, as well as their ratio R_{32}. These corrections are calculated from the leading order HERWIG++ with the default tune of version 2.3 (red line) and PYTHIA6 with tune Z2* (blue line); and the next-to-leading order POWHEG interfaced to PYTHIA8 with tune CUETS1 (green line) Monte Carlo event generators. The black solid circles give the average NP correction factor along with the uncertainty shown by the error bars.

6.1.3 Electroweak Corrections

At LHC, the center-of-mass energy of proton-proton collisions is well beyond the electroweak (EW) scale $\sim \mathcal{O}(100$ GeV). At such a high energy, the impact of higher order EW corrections is not any more negligible with respect to QCD effects [120] and affects the jet cross-sections at large $H_{T,2}/2$. The quark-quark scattering processes involving virtual exchanges of massive W and Z bosons contribute to electroweak (EW) corrections. The fixed-order QCD calculations do not include EW corrections and hence the NLO theory calculations are corrected for EW effects. The

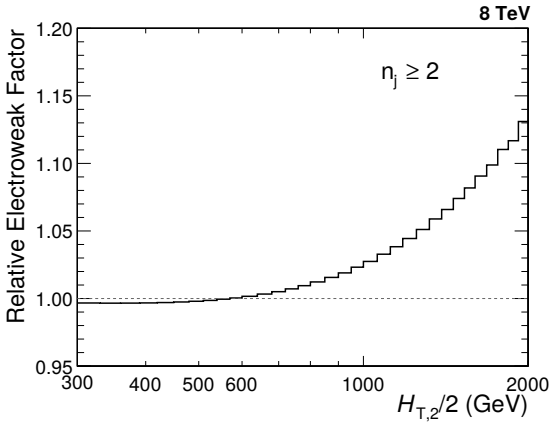

Figure 6.3: The electroweak (EW) corrections [121] in the phase space of the measurement are shown as a function of $H_{T,2}/2$ for inclusive 2-jet event cross-sections. These corrections are applied as a bin-by-bin correction factor to the fixed-order calculation of NLOJET++ as well as the MC predictions of MADGRAPH5+PYTHIA6. The EW correction factors increase up to 13% at high end of $H_{T,2}/2$ and significantly improves the agreement between data and prediction.

EW corrections have been calculated for inclusive 1-jet and 2-jet case, in Ref. [121]. The EW correction factors in the phase space of the measurement are shown as a function of $H_{T,2}/2$ in Fig. 6.3 for inclusive 2-jet event cross-sections. These correction factor increases up to 13% at high end of $H_{T,2}/2$ which are applied as bin-by-bin correction factors to the fixed-order NLOJET++ calculations. To see the effects of EW corrections, a ratio of the data to theory predictions obtained using CT10-NLO PDF set and corrected with NP effects without including EW corrections (left) and including EW corrections (right) is plotted for inclusive 2-jet event cross-sections in Fig. 6.4. On comparing both figures, it is observed that the EW corrections significantly improve the agreement between data and prediction in the high $H_{T,2}/2$ region. EW corrections are not available yet for inclusive 3-jet production and hence not applied for inclusive 3-jet event cross-sections. The guess from theory side is that EW for inclusive 2-jet and 3-jet will be similar, so for R_{32}, it is assumed to be equal to a factor of 1. Since the EW effects are not taken care of in MC simulations, these corrections are also applied to the MC predictions.

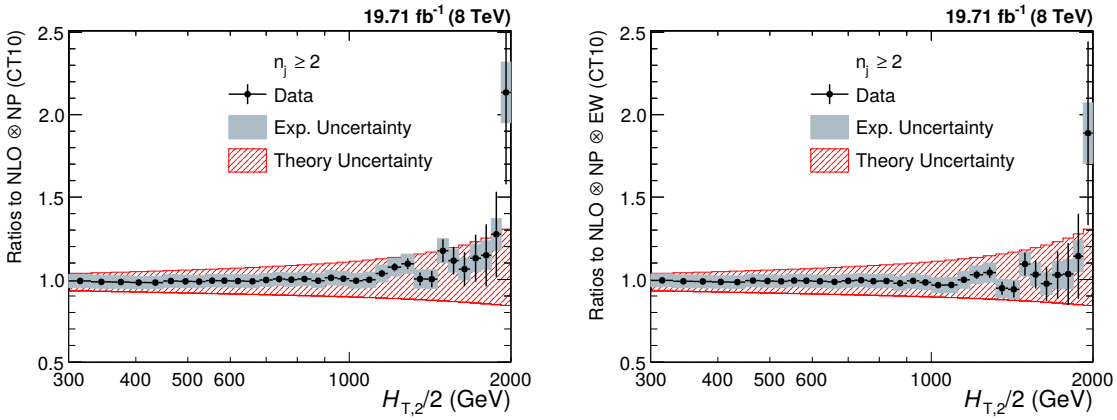

Figure 6.4: Ratio of the data over theory obtained using the CT10-NLO PDF set and corrected with non-perturbative effects (NP) without including electroweak (EW) corrections (left) and including EW corrections (right) is shown for inclusive 2-jet event cross-sections. The error bars represents the statistical uncertainty of the data and the shaded rectangles represents the total experimental systematic uncertainty. The shaded band around unity indicate the total uncertainty of the theory. The EW corrections significantly improve the agreement between data and prediction in the high $H_{\mathrm{T},2}/2$ region.

6.2 Theoretical Uncertainties

The measured differential inclusive multijet event cross-sections are not only sensitive to experimental uncertainties but also to the theoretical uncertainties. The renormalization and factorization scale variations, PDF uncertainties and the non-perturbative corrections contribute to theoretical uncertainties. These are described below :

6.2.1 Scale Uncertainty

In pQCD calculations of cross-sections, one has to choose a renormalization (μ_r) and factorization (μ_f) scale. The dependence on scales is negligible if these calculations are performed for all orders of the perturbative series, given by Eq. 2.8. Since the NLO describes this series up to second power in α_S, it introduces a scale dependence of the measurement which is covered by systematic uncertainty known as scale uncertainty. The scale uncertainty is evaluated with the conventional recipe of varying the default scale $H_{\mathrm{T},2}/2$ chosen for μ_r and μ_f independently in the following

six combinations: ($\mu_r/H_{\mathrm{T},2}/2$, $\mu_f/H_{\mathrm{T},2}/2$) = (1/2,1/2), (1/2,1), (1,1/2), (1,2), (2,1) and (2,2). The maximal upwards and downwards deviations in cross-section from the central prediction, give the scale uncertainty. To calculate the scale uncertainty for cross-section ratio R_{32}, firstly R_{32} is obtained for each of the above mentioned scale choices and then its difference from central R_{32} is taken. The scale uncertainty calculated using CT10-NLO PDF set ranges from 5% to 13% and 11% to 17% for inclusive 2-jet and 3-jet events cross-sections respectively, and from 6% to 8% for R_{32}.

6.2.2 PDF Uncertainty

The calculation of jet cross-sections in proton-proton collisions relies upon the knowledge of PDFs. These PDF sets are obtained by global fits to all the available deep inelastic scattering (DIS) and related hard scattering data from different experiments. The various sources affect the PDFs such as the theory model, input parameters like the strong coupling constant α_S, the quark masses and the statistical and systematic uncertainty sources of the data included in the PDF fit. These sources contribute to PDF uncertainty which is evaluated according to the prescriptions given for each PDF set. The CT10-NLO PDF set [115, 122] employs the eigenvector method to evaluate the PDF uncertainties. The CT10-PDF set consists of $N_{\mathrm{ev}} = 26$ eigenvectors with two PDF members per eigenvector k, which are varied upwards and downwards to generate a set of eigenvector pairs. The asymmetric uncertainties, ΔX^+ and ΔX^-, of a quantity X are given by Eq. 6.4 where X_0 is the central prediction, X_k^+ and X_k^- are the predictions using the upwards and downwards variation of each eigenvector k.

$$\Delta X^{+} = \sqrt{\sum_{k=1}^{N_{\text{ev}}} \left[\max(X_k^{+} - X^0, X_k^{-} - X^0, 0)\right]^2}$$
$$\Delta X^{-} = \sqrt{\sum_{k=1}^{N_{\text{ev}}} \left[\min(X_k^{+} - X^0, X_k^{-} - X^0, 0)\right]^2} \tag{6.4}$$

The symmetric uncertainty ($\Delta X^{\pm}$) is given by half the difference of the upwards and downwards variations :

$$\Delta X^{\pm} = \sqrt{\sum_{k=1}^{N_{\text{ev}}} \left[\frac{X_k^{+} - X_k^{-}}{2}\right]^2} \tag{6.5}$$

The CT10-NLO PDF set uncertainties are downscaled by a factor of 1.64 in order to have the uncertainties at the 68.3% confidence level CL(1σ) instead of 90% CL(2σ) such that to have a uniform treatment with respect to other PDF sets. The PDF uncertainty as derived with the CT10-NLO PDF set is the dominant source of uncertainty and ranges from 3% to 30% for inclusive 2-jet and from 4% to 32% for 3-jet cross-sections. For R_{32}, the ratio of predictions for inclusive 3-jet to that of 2-jet is taken for each eigen vector with upwards and downwards variations separately and then PDF uncertainty is calculated as done for individual cross-sections. The PDF uncertainty ranges and from 2% to 10% for cross-section ratio R_{32}.

6.2.3 Non-perturbative Uncertainty

As discussed in 6.1.2, the differences in the non-perturbative (NP) corrections calculated from various Monte Carlo event generators introduce the NP uncertainty which is of the order of 1% and 1 to 2% for inclusive 2-jet and 3-jet event cross-sections respectively, and $< 1\%$ for cross-section ratio R_{32}.

6.2.4 Total Theoretical Uncertainty

The total systematic theoretical uncertainties are obtained as the quadratic sum of the scale, PDF and NP uncertainties. Figure 6.5 presents the systematic theoretical uncertainties affecting the cross-section measurement for inclusive 2-jet (top left) and 3-jet (top right) events and the cross-section ratio R_{32} (bottom), using CT10-NLO PDF set. The scale (red dashed line), PDF (green line) and NP (blue dashed line) uncertainties as well as total theoretical uncertainty (black dashed line) are shown. The total theoretical uncertainty is asymmetric and dominated by PDF uncertainty which grows in magnitude with increasing value of $H_{T,2}/2$. Table 6.2

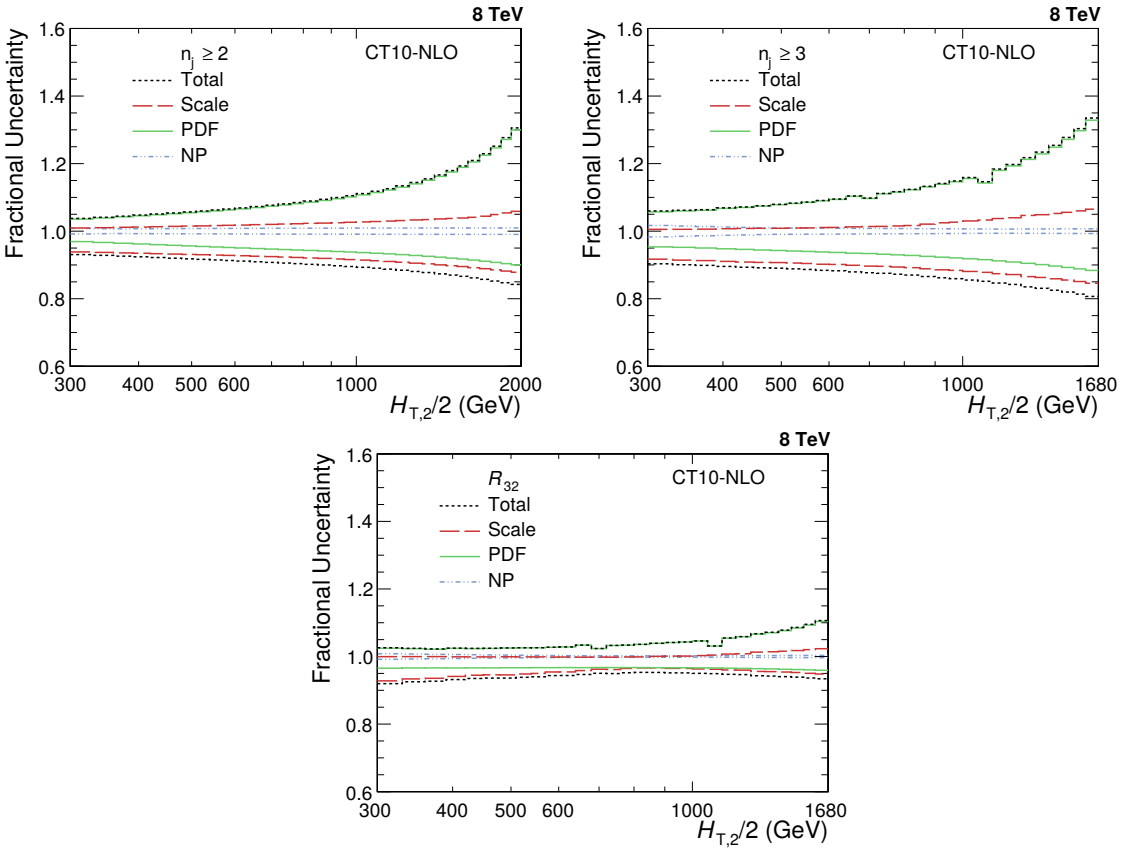

Figure 6.5: The systematic theoretical uncertainties affecting the cross-section measurement for inclusive 2-jet (top left) and 3-jet (top right) events and their ratio R_{32} (bottom). The scale (red dashed line), PDF (green line) and NP (blue dashed line) uncertainties as well as total uncertainty (black dashed line) obtained using CT10-NLO PDF set are shown. The total theoretical uncertainty is asymmetric and dominated by PDF uncertainty.

quotes the values of the theoretical uncertainty from each source as well as total uncertainty affecting the measurements. The bin-wise values of uncertainties (in %) from each source as well as total uncertainty are shown in Tables A.5, A.6 and A.7 for $n_j \geq 2$ and $n_j \geq 3$ event cross-sections and the cross-section ratio R_{32}, respectively. The computation of the NLO predictions with NLOJET++ is also subject to statistical fluctuations from the complex numerical integrations. For the inclusive 2-jet event cross-sections this uncertainty is smaller than about a per mille, while for the inclusive 3-jet event cross-section it amounts to 1-9 per mille. The small dips at ∼700 and 1000 GeV in the PDF uncertainty for inclusive 3-jet events cross-sections and the cross-section ratio R_{32} is a feature of the CT10-NLO PDF set.

Table 6.2: Overview of all systematic theoretical uncertainties, obtained using CT10-NLO PDF set, affecting the measurement of cross-sections for inclusive 2-jet (left) and 3-jet (middle) events and the cross-section ratio R_{32} (right).

Uncertainty Source	**Inclusive 2-jet**	**Inclusive 3-jet**	$\boldsymbol{R_{32}}$
Scale	5 to 13%	11 to 17%	6 to 8%
PDF	3 to 30%	4 to 32%	2 to 10%
Non-perturbative (NP)	1%	1 to 2%	$< 1\%$
Total	3 to 30%	5 to 34%	3 to 11%

6.3 Comparison of Theory to Data

After correcting the measurement for detector effects as well as NLO pQCD calculations for non-perturbative (NP) and electroweak (EW) effects, it is now feasible to compare the measured cross-sections with the theory predictions. Figure 6.6 shows the measured differential inclusive 2-jet and 3-jet event cross-sections as a function of $H_{T,2}/2$ after unfolding for detector effects. On the left, the measurements (points) are compared to the NLOJET++ predictions using the CT10-NLO PDF set (line), corrected for NP effects and in addition for EW effects in the 2-jet case. On the right,

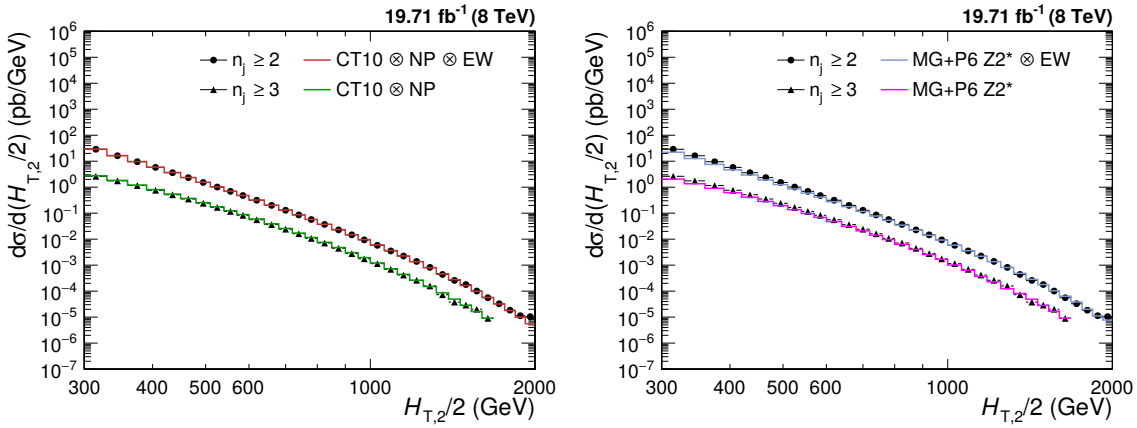

Figure 6.6: Comparison of the measured differential inclusive 2-jet and 3-jet event cross-sections as a function of $H_{T,2}/2$ to theoretical predictions. On the left, the data (points) are shown together with NLOJET++ predictions (line) using the CT10-NLO PDF set, corrected for non-perturbative (NP) and electroweak (EW) effects (2-jet) or only NP effects (3-jet). On the (right), the data (points) are compared to predictions from MADGRAPH5+PYTHIA6 (MG+P6) with tune Z2* (line), corrected for EW effects in the 2-jet case. The error bars give the total experimental uncertainty, given by the quadrature sum of the statistical and systematic uncertainties.

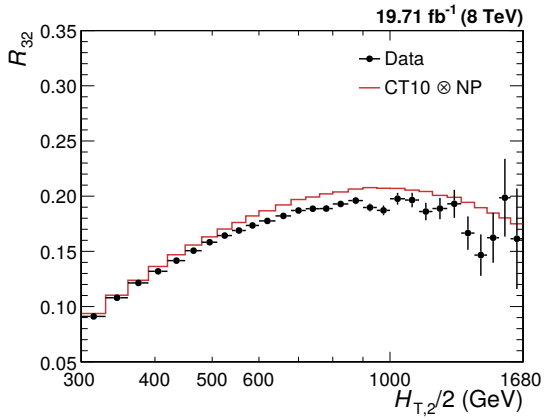

Figure 6.7: Cross-section ratio R_{32} as a function of $H_{T,2}/2$ calculated from data (solid circles) in comparison to that from NLO pQCD predictions obtained using the CT10-NLO PDF set corrected with non-perturbative (NP) corrections (line). The error bars correspond to the total experimental uncertainty derived as quadratic sum from all uncertainty sources.

the comparison is made to the predictions from MADGRAPH5+PYTHIA6 (MG+P6) with tune Z2* (line), corrected for EW effects in the 2-jet case. The error bars give the total experimental uncertainty, given by the quadrature sum of the statistical and systematic uncertainties. On a logarithmic scale, the data are in good agree-

ment with the NLO predictions over the whole range of $H_{\mathrm{T},2}/2$ from 300 GeV up to 2000 (2-jet) and 1680 GeV (3-jet) respectively.

Figure 6.7 shows the cross-section ratio R_{32} obtained from unfolded data (solid circles) in comparison to that from NLO pQCD predictions obtained using the CT10-NLO PDF set corrected with NP corrections (line). The error bars here represent the total experimental uncertainty derived as quadratic sum from all uncertainty sources. The deviations of measured R_{32} from the predicted theoretical value can be explained by the electroweak effects which are not considered yet because of their unavailability for inclusive 3-jet event cross-sections.

For better comparisons, the ratios of the data over the theory at NLO are also studied in detail. In Fig. 6.8, the ratios of the data over NLOJET++ predictions using the CT10-NLO PDF set are shown for inclusive 2-jet (top left) and 3-jet (top right) event cross-sections as well as their ratio R_{32} (bottom). The data are well described by the predictions within their uncertainties, which are dominated at large $H_{\mathrm{T},2}/2$ by PDF effects in the upwards and by scale variations in the downwards direction. A trend towards an increasing systematic excess of the 2-jet data with respect to theory, starting at about 1 TeV in $H_{\mathrm{T},2}/2$, is remedied by the inclusion of EWK corrections. In the 3-jet case the statistical precision of the data and the reach in $H_{\mathrm{T},2}/2$ is insufficient to observe any effect. The alternative PDF sets MSTW2008 and NNPDF2.3 exhibit a small underestimation of the cross-sections at high $H_{\mathrm{T},2}/2$.

The POWHEG framework providing the NLO dijet calculation matched to the parton showers of PYTHIA8 employed with the CUETS1 and CUETM1 tunes [78] is also used for a comparison. The ratios of the data w.r.t. theory from POWHEG+PYTHIA8 with tune CUETS1 are shown for inclusive 2-jet (top left) and 3-jet (top right) event cross-sections as well as their ratio R_{32} (bottom) in Fig. 6.9. For comparison, the LO prediction from PYTHIA6 with tune Z2*, the tree-level multi-leg improved prediction by MADGRAPH5+PYTHIA6 with tune Z2*, and the matched

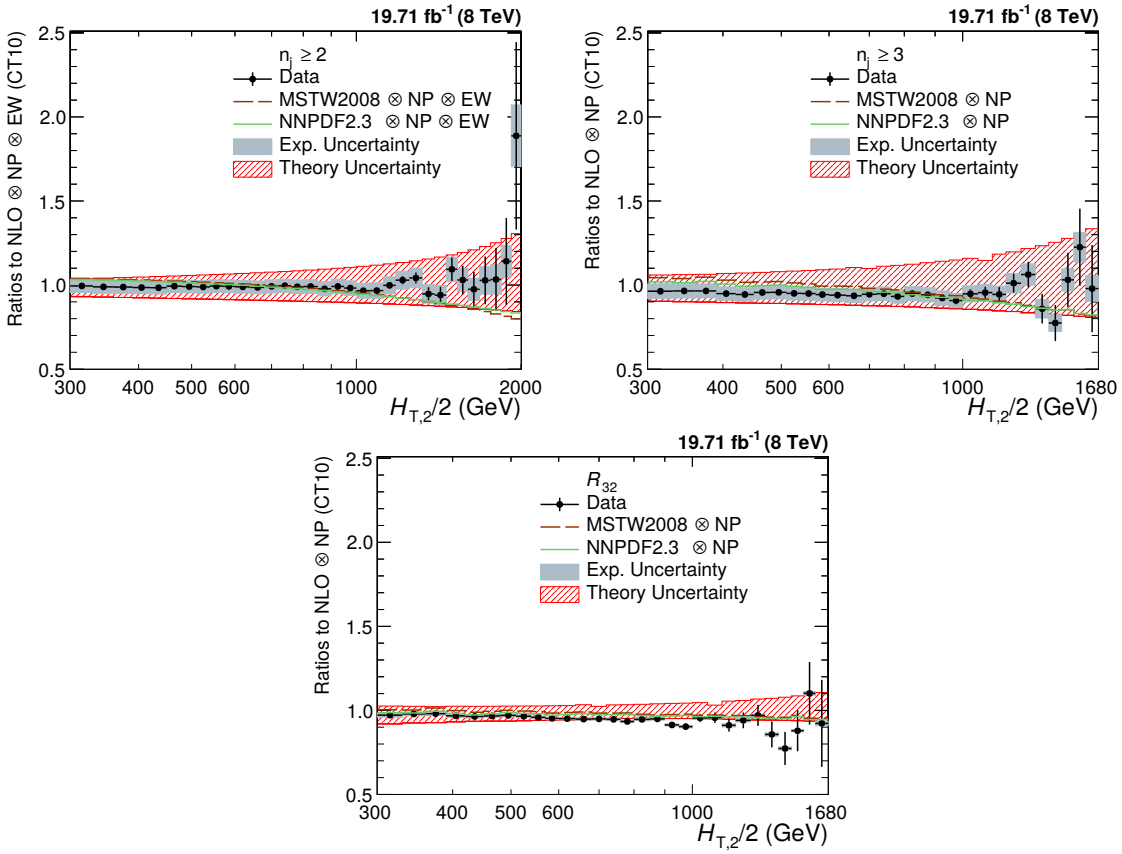

Figure 6.8: Ratio of the data over theory using the CT10-NLO PDF set for inclusive 2-jet (top left) and 3-jet (top right) event cross-sections and their ratio R_{32} (bottom). The theory predictions are corrected for non-perturbative effects (NP) and also for electroweak effects (EW) for inclusive 2-jet only. For comparison predictions employing two other PDF sets, MSTW2008 and NNPDF2.3, are also shown. The error bars represent the statistical uncertainty of the data and the shaded rectangles represents the total experimental systematic uncertainty. The shaded band around unity indicate the total uncertainty of the theory.

NLO prediction from POWHEG+PYTHIA8 with tune CUETM1 are shown as well. EW corrections have been accounted for in this comparison for the 2-jet case only. Significant discrepancies, which are cancelled to a large extent in the ratio R_{32}, are visible in the comparison with the LO prediction from MADGRAPH5+PYTHIA6 with tune Z2*, in particular for small $H_{T,2}/2$. In contrast, the employed dijet MC POWHEG+PYTHIA8 better describe the 2-jet event cross-section, but fail for the 3-jet case.

The jet measurements at hadron colliders can be used to extract the strong coupling constant α_S, which is discussed in the next chapter.

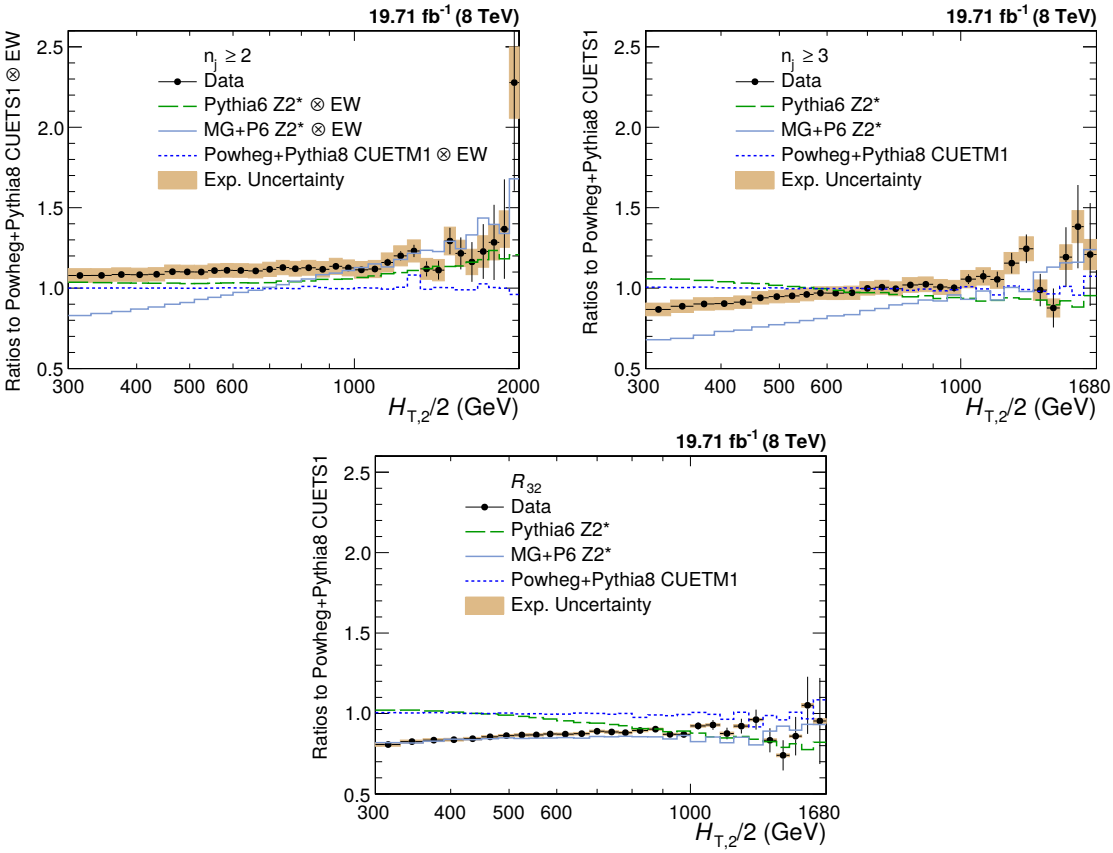

Figure 6.9: Ratio of the data over the predictions from POWHEG+PYTHIA8 with tune CUETS1 are presented for inclusive 2-jet (top left) and 3-jet (top right) event cross-sections as well as their ratio R_{32} (bottom). For comparison the alternative tune CUETM1 of POWHEG+PYTHIA8, the tree-level multi-leg improved prediction by MADGRAPH5+PYTHIA6 with tune Z2*, and the the LO MC predictions from PYTHIA6 tune Z2* are shown as well. The error bars correspond to the statistical uncertainty of the data and the shaded rectangles to the total experimental systematic uncertainty. EW corrections have been accounted for in this comparison for the 2-jet case only.